Design and Modeling of Electrohydrodynamically-driven Droplets for Fluid Joints Microactuators

Francisco Ortiz*, Aude Bolopion and Antoine Barbot

Abstract—**Microscale actuation holds transformative potential across various fields by enabling precise and minimally invasive actions, however downsize actuators while keeping relative large actuation range is challenging. Electrohydrodynamics (EHD) forces, arising from electric field-fluid interaction, can greatly deform fluid surface at microscale, yet there is a lack of knowledge regarding the modeling, control, and specificity which hinder their use in microactuator designs. This work, aims to design, model and open-loop control a droplet driven by EHD, focusing on its application in fluid joints (i.e. two solids link together by a liquid droplet) based microactuators. The model merges an energy-based steady-state hysteresis with linear dynamics, using the steady-state inverse as an open-loop controller to control the droplet's height. For a selected design, both steady-state and dynamic models were fitted using a 3μL droplet of glycerin and the control strategy was tested. The model accurately predicts the stable droplet position, while the control strategy maintains a height error under 14 μm, a motion amplitude of 150 μm, and high repeatability. This work contributes to the advancement of microscale actuation by presenting a model and open-loop control strategy for EHD-driven droplets, facilitating practical use as a microactuator for fluid joints in microrobotic applications.**

Index Terms—**Microrobotics, Electrowetting, Electrohydrodynamics, Control, Fluid Joints, Open-Loop Control**

I. INTRODUCTION

MICROSCALE robot actuation is important to enable precise, minimally invasive actions at the microscale, leading to advancements in medicine, manufacturing, environmental monitoring, and more. This small scale actuation is challenging due to the shifting dominance of physical laws depending on the system scale. This variability in the predominant forces complicates the downsizing of macro-actuators such as motors. In particular, in the microworld (size $< 1 \times 10^{-3}$ m), surface tension forces become predominant. This predominance of surface tension forces makes them attractive for microrobotics applications such as microassembly [1], pick-and-place grippers [2]–[4], and microrobot displacement [5], [6], to name a few.

To actuate capillary forces, five principal approaches have been identified [7], by controlling the pressure difference between the liquid and the environment [8], [9], controlling the volume of the meniscus [4], [10], generating a flow inside the meniscus [11], [12], acting on the contact angle [13], [14] and using a volume force on the fluid to change the shape of the meniscus [15], [16].

The use of electric fields to change the contact angle, which is based on ElectroHydroDynamics (EHD) effects, offers interesting advantages with low power consumption [17]. Unlike magnetic actuation, electric actuation embeds the actuation principle within the device, reducing the size of the device and increasing its compactness (the ratio between the actuator range of motion and actuator size) [18]. Additionally, it offers the potential for internal sensing by utilizing the electrodes to measure the electrical properties [19], which can improve the accuracy of the actuator by providing feedback. Furthermore, this actuation not only provides the possibility of symmetrically deforming a droplet as in [20] where a microgripper with a gripped object floating on it is presented, but complex 3D shapes can also be achieved as demonstrated in [13], where a droplet with a plate on its surface is deformed in 3D to obtain a rotary motion. However, it also presents several challenges, such as modeling and control, in particular due to the nonlinear and hysteresis behavior of the wetting-dewetting cycle.

Incorporating theoretical models for actuator response proves beneficial in the design process, offering predictions of system behavior before fabrication and enabling precise control during actuation. EHD actuation has been well modeled to predict the change in the contact angle as well to analyze the stability position of the droplet. For instance, in [21], the stability position of the droplet is assessed by maximizing the capacitance, treating the droplet as a complete plate electrode and a grounded device, although not considering surface changes and hysteresis in the contact angle. In [22], the droplet dynamics is investigated and a non-linear model based on the contact angle is derived. In [23], a model of the steady-state behavior of a droplet driven by EHD, accounting for contact angle hysteresis, is successfully tested.

However, existing models are limited, typically focusing on predicting either droplet stability or changes in the contact angle individually. These models are constrained by specific electrode shapes, and the effectiveness of control strategies remains unverified. Moreover, proposed devices often function as proofs of concept without accompanying control strategies. Consequently, microactuator designers require the development of models that provide the freedom to alter electrode shapes to achieve the desired behavior. Additionally, as demonstrated in [24], droplets can serve as actuated fluid joints. Nonetheless, before integrating them into complex

Authors are with FEMTO-ST Institute, AS2M department, Univ Bourgogne Franche-Comté, CNRS, 24 rue Alain Savary, 25000 Besancon, France, *francisco.ortiz@femto-st.fr*

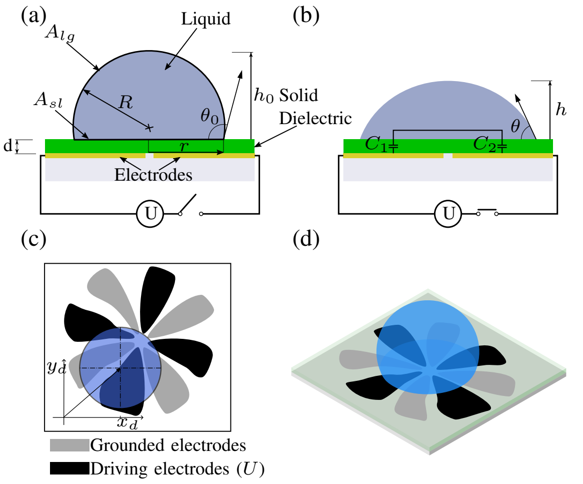

Fig. 1. Schematics of a droplet actuated by Electrohydrodynamics forces along with the proposed model. (a) The droplet is in its non-powered stable position, where A_{lg} and A_{sl} represent the liquid-gas and solid-liquid areas, θ_0 is the initial contact angle, h is the height, R is the radius of the droplet, and d is the thickness of the dielectric layer. (b) When a voltage is applied, the droplet's shape changes, and both the contact angle and the height of the droplet are reduced. C_1 and C_2 denote the capacity of the model, and U is the applied voltage. (c) Top view of the EHD device with the droplet on the surface and x, y represent the position of the droplet. (d) 3D illustration of a typical EHD device device.

devices, it is crucial to effectively model and control isolated droplets. Additionally, key attributes for actuators in microrobotics include motion repeatability and predictability. The actuator's steady-state and dynamic responses are crucial for understanding system behavior, facilitating automation and control, and ensuring effective microrobot performance in designated tasks.

In this work, we propose a model to design and predict the steady and dynamic behavior of a droplet driven by EHD actuation, with focus in the application to fluid joints control. In addition, we propose an open-loop control strategy based on the inverse model of the steady-state response for the height of the droplet. We present the design process of the actuators, as well as the characterization and extraction of their most important characteristics required for a control model. This design provides 1D deformation, which can serve as both a linear actuator as well as a fluid joint by placing an object in the surface of the droplet. Moreover, it offers self-centering behavior of the droplet. Additionally, we validate the proposed control strategy through experiments to test its functionality and accuracy.

This article is structured as follows. Section II describes the principle of EHD actuation. Section III presents the characterization of devices driven by EHD, including steady-state and dynamic modeling, and then the experimental results are presented and discussed. Section IV covers the open-loop control strategy and presents the corresponding experimental results. Finally, Section V concludes the article.

II. PRINCIPLE OF ELECTROHYDRODYNAMICS ACTUATION

Electrohydrodynamics (EHD) can be considered as the dynamics of a fluid in an electrical field [25], and the forces exerted on the liquid by the electric field can be described by the Korteweg-Hemholtz body force density [26]

$$\vec{f}_k = \rho_f \vec{E} - \frac{\epsilon_0}{2} E^2 \nabla \epsilon + \nabla \left[\frac{\epsilon_0}{2} E^2 \frac{\partial \epsilon}{\partial \rho} \rho \right] \qquad (1)$$

where ρ and ϵ are the mass density and the dielectric constant of the liquid, respectively, ρ_f is the free electric charge density of the fluid, ϵ_0 is the vacuum permittivity, and E the electrical field. The last term of the equation describes electrostriction and can be neglected for incompressible fluids, as in our study. By examining this equation, we can identify two extreme scenarios. In the first scenario, the liquid is dielectric ($\rho_f = 0$ and $\nabla \epsilon \neq 0$) this phenomenon is known as dielectrowetting (DEW) [27], with the forces being volume forces. The second scenario when the liquid is a perfect conductor (ρ_f and $\nabla \epsilon$ are zero within the bulk, and $\rho_f = \rho_s$ at the surface, also $\nabla \epsilon \neq 0$ at the interface due to the inhomogeneity of permittivity of the two different mediums), it is referred as electrowetting (EW) [26] and with the forces being superficial. Additionally, the electrical properties are frequency-dependent. Thus, the actuation dominance by either EW or DEW, or a combination of both, is determined by the liquid properties and the frequency of the applied signal.

This effect can be observed in liquid droplets in devices such as the one illustrated in the figure 1. The device consists of a droplet placed on a dielectric layer covering two sets of electrodes, which generate the electric field by being powered with a voltage source. When the switch is turned on (Figure 1 (b)), an electric field is generated which impact the droplet shape. This results in a change of the wetting between the liquid droplet and the surface described by the contact angle θ.

A particular characteristic of this type of device is that, when a voltage is applied, the droplet can move on the substrate due to unbalanced forces over the triple contact line, where the liquid-solid-air interfaces intersect. This is an issue to make an actuator where only the height of the droplet change while its center remain at the same position, and therefore must be taken into account. In addition, EHD actuation presents nonideal behavior for control, such as contact angle hysteresis. The contact angle hysteresis is defined as the difference between the advancing and receding contact angles and it is mainly attributed to surface roughness and chemical heterogeneities [28]. This behavior occurs in EHD when the transition between wetting and dewetting regimes (and vice versa) results in a hysteresis of the contact angle (θ) value with variation of the applied voltage (U).

III. DESIGN AND CHARACTERIZATION OF EHD ACTUATED DROPLET DEVICE

Characterization of the device includes the stable droplet positioning, steady-state and dynamic droplet height changes with the voltage applied, and models and experimental setup to validate them.

A. Experimental setup

The experimental setup included two cameras with dedicated microscope objectives for top and side views, recording

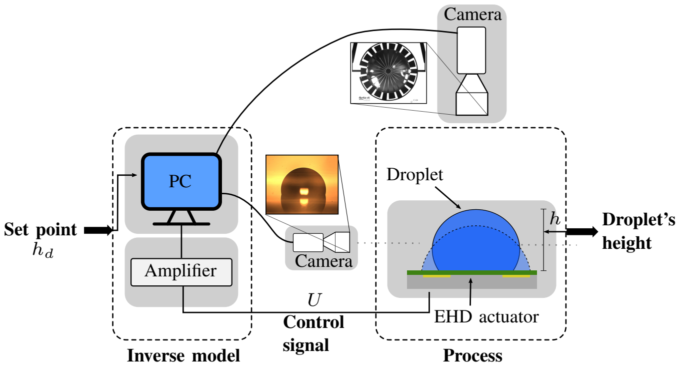

Fig. 2. Schematics of the experimental setup. It consists of side and top view cameras and a voltage signal generator.

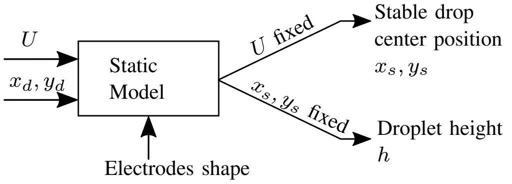

Fig. 3. The static model predicts the drop center position and its height. U is the voltage applied, x_d,y_d are the coordinates of the droplet, x_s,y_s are the coordinates of the stable position of the droplet and h is the droplet height.

images on a computer at 30 fps, as shown in Figure 2. To actuate the system, two sinusoidal signals with identical amplitudes and a 180-degree phase shift were generated using a computer and a DAQ (Data Acquisition) board.

The fluid used for the fluid joints influences its performance. Due to the use of air-solid-liquid interfaces, the EHD actuation only enables the reduction of contact angle, making higher initial contact angles preferable. In addition, the output force of the device is proportional to the surface tension of the fluid [29], while the evaporation rate is crucial to prevent the reduction of the droplet size and ensure repeatability [30]. Glycerin was used as working fluid to mitigate evaporation and to have a high surface tension and initial contact angle. The deposition of 3 μL droplets was carried out using a droplet dispenser. To minimize volume changes resulting from the hygroscopic nature of glycerine, we waited overnight to reach equilibrium before conducting experiments, resulting in a stable mixture of glycerin and water with a high surface tension and contact angle. After data acquisition, data analysis was performed using pyDSA software [31], where the height of the droplet was determined by approximating the shape of its side view as an ellipse.

The electrode fabrication process begins with a glass substrate in which a Cr/Au (15/200 nm) layer was deposited by evaporation and patterned by lithography. Then a layer of pure CTL-809L Cytop® was deposited by spincoating (3000 RPMs during 20 seconds) and baked at 200° during 1 hour, obtaining a 900 nm thick layer.

B. Static Behavior

To model horizontal position and the height of the droplet, we propose an energy-based model (Figure 3), which takes as inputs the applied voltage and the position of the droplet, and, through energy minimization, provides the stable droplet position and droplet height for a given geometry of electrodes.

1) Static Model: Let's consider the device in Figure 1, which consists of two arrays of electrodes: one with voltage U and the other grounded, covered by a dielectric of thickness d. The droplet is considered as a spherical cap of perfect conductor liquid, implying the electrowetting regime, and its position is determined by the coordinates of its center, x_d and y_d (as defined in Figure 1(c)). The perfect conductor assumption is valid when the dielectric constant of the fluid exceeds that of the dielectric layer. For glycerine-cytop, this ratio is greater than 20, and for water-cytop, it is greater than 35.

The energy of the system is calculated as the sum of the interfacials energy, the electrical energy and the energy due to the pinning of the contact line:

$$E = E_{surf} + E_{pin} + E_{elec}. \tag{2}$$

The first term is calculated as $E_{surf} = (\gamma_{sl} - \gamma_{sg})A_{sl} + \gamma_{lg}A_{lg}$, where γ_{sl}, γ_{lg}, A_{sl} and A_{lg} are the solid-liquid, liquid-gas interfacial tensions, the solid-liquid and the liquid-gas surface areas respectively. Moreover, assuming the droplet is a spherical cap, the surface energy can be written using the geometry of the droplet (Fig. 1, [32]):

$$E_{surf} = \pi^{1/3}(3V)^{2/3}\left(\gamma_{sl}\frac{sin^2\theta}{f(\theta)^{2/3}} + 2\gamma_{gl}\frac{1-cos\theta}{f(\theta)^{2/3}}\right) \tag{3}$$

with $f(\theta) = (2 + cos\theta)(1 - cos\theta)^2$.

The electrical energy E_{elec} is calculated as the difference between the storage of energy of the capacitor and the given energy of the power source [33], $E_{elec} = -1/2CU^2$, where C is the capacitance of the system and U the voltage applied. This capacitance was approximated by considering the system as two electrodes connected to a voltage source U, covered by a dielectric layer with thickness d and the droplet placed over it, as shown in Figure 1 (b). This configuration was simplified as two parallel plates capacitors in serie ($C_1 = A_1\frac{\epsilon_0\epsilon_d}{d}$ in series with $C_2 = A_2\frac{\epsilon_0\epsilon_d}{d}$), where ϵ_0 and ϵ_d are the permittivity of free space and the dielectric constant of the dielectric layer, and A_1 and A_2, are the two electrode areas covered by the droplet, respectively. Here it is important to notice that both areas depends on the geometry of the electrodes, the radius and position of the droplet, $(A_1(r, x_d, y_d), A_2(r, x_d, y_d))$. In addition to the ideal model described above, the constants C_g^{adv} and C_g^{rec} have been incorporated into the electrical energy model for both the advancing and receding regimes. These constants compensate for the simplifications we have made and allow the extension of the model for an alternative voltage source using the root mean square value, U_{rms}. Additionally, they consider different sensitivities to voltage changes during the advancing and receding regimes. This leads to the derivation of equation (4).

$$E_{elec} = \begin{cases} \dfrac{-\epsilon_0\epsilon_d}{2d}\dfrac{C_g^{adv}}{1/A_1 + 1/A_2}U_{rms}^2, & \text{if U increases.} \\ \dfrac{-\epsilon_0\epsilon_d}{2d}\dfrac{C_g^{rec}}{1/A_1 + 1/A_2}U_{rms}^2, & \text{if U decreases.} \end{cases} \tag{4}$$

Finally, the pinning energy E_{pin} was calculated in a similar way as in [23]. This involves dividing the actuation in the advancing and receding regime, whether the voltage is increasing or decreasing, and also dividing each regime into two parts, whether the triple contact line is moving or not. To identify the regime in which the triple contact line is either moving or not, two voltage thresholds, Δu_1 and Δu_2, were defined—one as the voltage needed to switch from dewetting to wetting regime and viceversa respectively, as shown in equation (5). The advancing regime is when the droplet spreads on the surface and thus the voltage U increases. In this regime, at the beginning when the voltage is increasing, the triple contact line is pinned because of static friction force f_{cl} [23], and the contact angle remains unchanged due to the spherical cap hypothesis. This means that in this regime the change in electrical energy is equal to the pinned energy ($f_{cl}A_{sl} = \Delta E_{elec}$). When the change in the voltage reaches the value Δu_1, the static friction force f_{cl} reaches it maximum c_{pin}, and the triple contact line begins to move triggering the second stage of the advancing regime. The receding regime is essentially the opposite of the advancing regime; in this case, the voltage is decreasing and the droplet dewetting. At the beginning when the voltage starts to decrease, the triple contact line is pinned and the contact angle remains unchanged. Once the voltage decrease up to the value ΔU_2, the triple contact line begins to recede.

$$E_{pin} = \begin{cases} f_{cl}A_{sl}, & \text{if U increases and } \Delta U < \Delta u_1. \\ c_{pin}A_{sl}, & \text{if U increases and } \Delta U > \Delta u_1. \\ -f_{cl}A_{sl}, & \text{if U decreases and } \Delta U < \Delta u_2. \\ -c_{pin}A_{sl}, & \text{if U decreases and } \Delta U > \Delta u_2. \end{cases} \tag{5}$$

The accuracy of the model is affected by the assumption of a spherical cap in Equation (3), which can lead to errors for droplets with radius close to or larger than the capillary length (2.2 mm for glycerin). Additionally, errors in determining the volume of the droplet directly affect height calculation with a relative error proportional to the volume error. Also the output forces can be influenced by changes in the volume of the droplet.

With this model defined, we can distinguish the two cases in Figure 3, one to analyze the stable position of the droplet and the other to obtain the change in the height of the droplet due to the voltage applied when it is in a stable position.

a) Case I: Droplet stable position: In the first case, if we assume the droplet shape remains approximately constant with the voltage, the terms E_{surf} and E_{pin} can be treated as a constant. Then, for the energy minimization , we only need to focus on extremes of the function:

$$F_g = \frac{1}{1/A_1 + 1/A_2} \tag{6}$$

The energy is minimized when this function is maximized (see (4)). As the shape of a droplet is approximated as a spherical cap, the function F_g depends on the position (x_d, y_d) and the radius (r) of the droplet's footprint, as well as the geometry of the electrodes. Therefore by computing F_g for different position, we can thus deduce the stable position x_d, y_d of the droplet as well as the region where the droplet will converge to this stable position when the current will be applied.

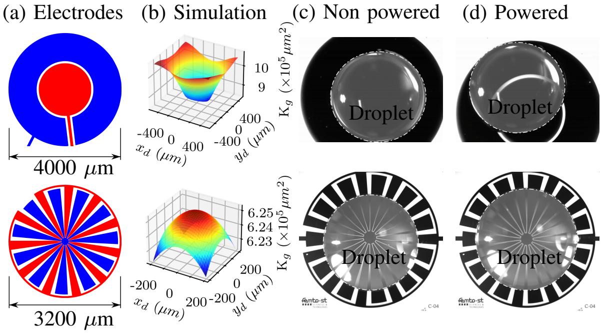

Fig. 4. Electrodes design and model validation. (a) Schematics of the electrodes design, red and blue indicates different polarities. (b) Simulations of the models. (c) Non-powered electrodes with droplets placed near the center of the electrodes. (d) Electrodes being actuated, in the top case the droplet moves to the side and in the bottom case, the droplets moves to the center.

b) Case II: Droplet height: In the second case, we assume that the center of the droplet is at a known stable position and that the droplet remains a spherical cap, but its height can be changed by the electric field. The height of the droplet for a given voltage can be calculated by minimizing the equation (2). In this case, all the terms, $E_{surface}$, E_{pin}, and E_{elec} must be calculated. Then, by finding the minimum energy, it is possible to determine the equilibrium value of θ for a given droplet volume and applied voltage. Finally, through geometry, h can be calculated.

To compute the energy and find the value of θ that minimized it, the analytical equation can be obtained if the areas A_1 and A_2, and therefore F_g have an analytical form. Since it is difficult to find the analytical equation for general electrodes designs, we calculated the values of the function F_g numerically, as well as the derivative of the energy. This approach not only enables us to compute the energy without requiring an analytical equation for the electrode shape, but also provides greater flexibility in designing electrodes and exploring various shapes using the proposed model.

2) Droplet centering: We investigated several electrode designs, but for simplicity, the results of only two of them are presented in Figure 4(a). We validated the centering model by comparing the prediction of the model with the experimental results. To calculate the function F_g, we have set a fixed droplet size and the position of interest as the center of the electrode. Then we calculated the areas covered by the droplet, A_1 and A_2, in the position of interest and also when the droplet was moved from the center a distance in the x and y directions. With these values, we calculated the function F_g for different droplet positions and plotted the values on a surface graph, which is shown in Figure 4 (b). There we can see that for the top design the stables positions (maximums of F_g) are located in the surroundings and for the bottom design, the stable position is in the center. The experimental results of these designs with powered and nonpowered electrodes are presented in Figures 4 (c) and (d), and confirm the model predictions.

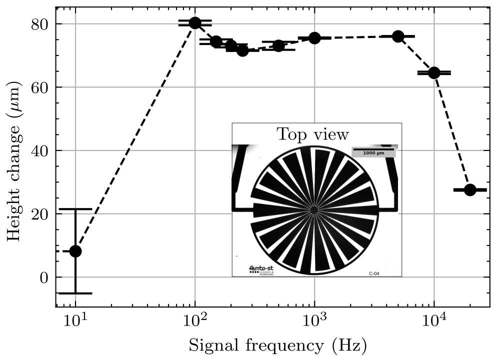

Fig. 5. Change in droplet (glycerine water mixture) height for a 40 V_{rms} step at various frequencies and top view of the stable centering electrode chosen in this work, black color corresponds to the gold.

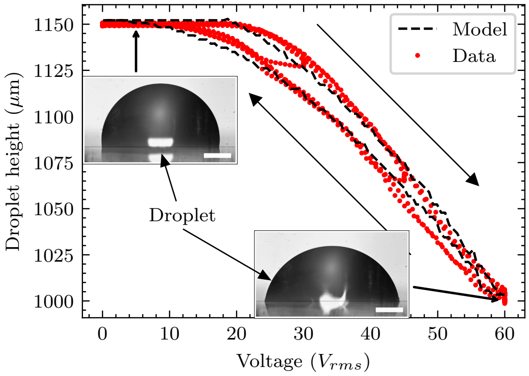

Fig. 6. Steady-state response of the system measured with two side view snapshots and model prediction (scale bar, 500 μm). The horizontal axis represents the voltage applied in V_{rms}, the vertical axis denotes the height of the droplet, and arrows indicates the evolutionary directions.

3) Actuator motion range and signal frequency dependence: As we showed in Section II, the electrohydrodynamic response of a fluid depends on the frequency of the input signal, therefore, the dependency of the range of motion must be explored. Notably, the driving frequency is expected to be dependent on the fluid rather than the size of the drop, due to the frequency-dependent electrical characteristics generally present in fluids. To characterize electrode actuation, shown in Figure 5, we measured droplet height changes while applying a square signal with a high voltage of 40 V_{rms} and a low voltage of 0 to the electrodes, with frequencies ranging from 0 to 20 kHz. The results are presented in Figure 5, where the error bars correspond to the standard deviation of the measurements. In this figure, we can see that at frequencies below 100 Hz the change in height is lower than 20 μm, then in the region between 100-5000 Hz the change in height is between 70-80 μm. Beyond 5000 Hz, the change in height decrease as the frequency increase. Therefore, the frequency range of 100-5000 Hz appears to be a suitable range to set the input signal frequency. In addition to the frequency dependence of the motion range, the mechanical resonance of the droplet must be taken into account. Despite the absence of resonance in Figure 5, the measurements were performed using a constant voltage and the resonance frequencies vary with θ [34], and thus with the applied voltage. Therefore, to mitigate resonances, we set a working frequency of 200Hz.

Additionally, the motion range will be affected when extracting forces using this device. To do so, it is necessary to connect the droplet with another object or plate where the forces will be applied. The size and shape of the connected object influence both the motion range and the output forces. This influence can be analyzed by simulating the fluid joint using Surface Evolver software [35]. For the case of using a circular plate as a connected object, it is possible to find that the larger the plate, the higher the forces, leading to forces of the order of hundreds of micronewton for plates of radius close to or greater than 1 mm. However, adding an object to the drop deforms it, and thus influences its height. Consequently, larger plates also result in lower equilibrium positions and reduced range of motion.

4) Steady-state response: Once the signal frequency was established, the static response of the system with the electrodes of Figure 5 was characterized. For this purpose, the height of the droplet was measured when applying 3 cycles of voltages ranging from 0-60, 0-45 and 0-30 V_{rms}, with a slope of 2 V/s. The results are depicted in red in Figure 6.

We can observe that there is a threshold of 20 V_{rms} required to initiate the actuation process, and the contact angle evolution to the applied voltage clearly exhibits a hysteresis behavior. This hysteresis is attributed to the contact angle hysteresis [23]. Additionally, the height of the droplet achieved falls within the range of 1150 to 1000 μm, representing a change in height of 13%. It is noteworthy that the advancing and receding curves are consistent across all three cycles.

The measured data of the first cycle, the bigger from 0 to 60 V_{rms}, was used to fit the energy model and determined the values of C_g^{adv}, C_g^{rec}, c_{pin}, in equations (4) and (5), and the equilibrium contact angle θ_0. The fitted parameters are $C_g^{adv} = 1.756$, $C_g^{rec} = 1.66$, $\theta_0 = 97.16°$ and $c_{pin} = 0.001$, and the data and the fit model are shown in black in Figure 6.

It confirms that the model matches the behavior of the steady-state response of the droplet's height. Additionally, the largest deviations of the model prediction are located at low and high voltages in the receding regime of the curve, and at voltages between 20 and 35 V_{rms} in the advancing regime. This error may arise from the assumption of the droplet as a spherical cap and the assumption that the liquid is a perfect conductor. Furthermore, the errors at low voltages indicate that there is a voltage thresholds in the receding part. This is consistent with the observations made in [36] and the model could be improved to take into account this threshold by changing U in equation (4) by $U - U_{th}$, where U_{th} is the voltage threshold. However, those deviations are less than 10 μm, and represent only 6.7% of the full range of actuation.

The static model predicts the droplet center stable position and its height; however, it does not capture the dynamics, which is the goal of the dynamic model presented in the next section.

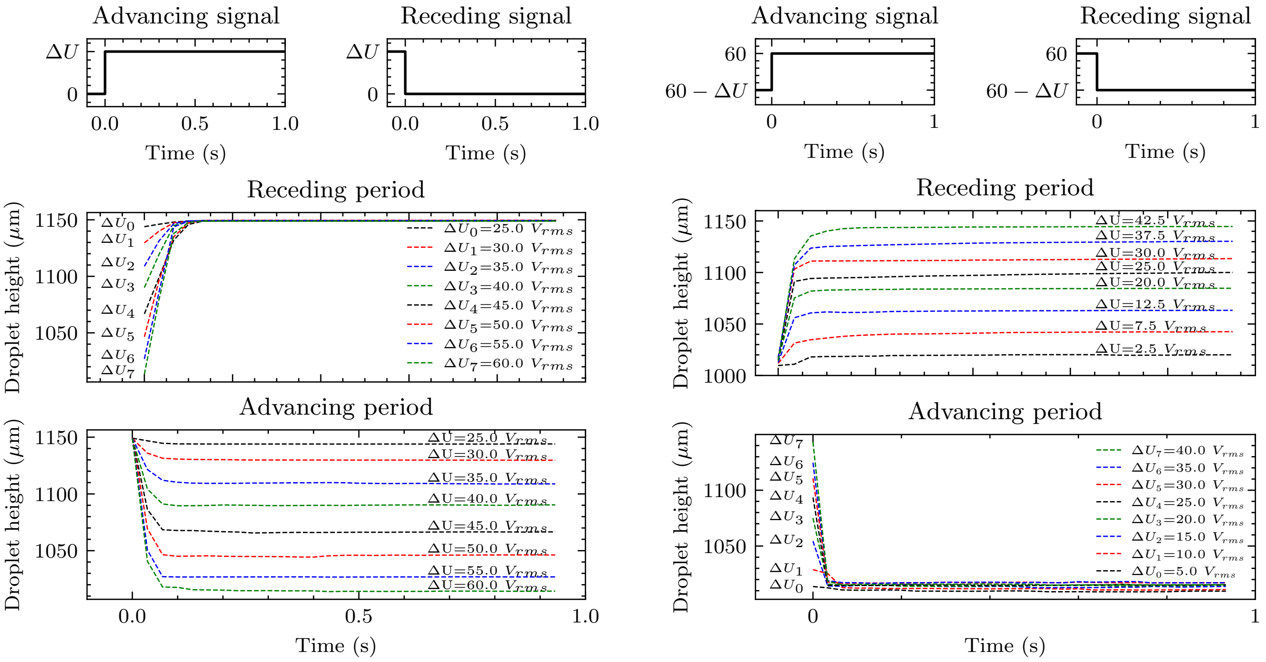

(a)

(b)

Fig. 7. Time response in the wetting and dewetting process with corresponding droplet height vs. time data. The top signal represents the actuation signal during the advancing and receding regimes. The vertical axis is the height and the horizontal axis is the step time in seconds. In all the cases tested, 90% of the steady state value is reached in less than 0.22 seconds. (a) Time response for a square signal with a low constant value of 0 V_{rms} and a high value varying from 0 to 60. (b) Time response for a square signal with a high constant value of 60 V_{rms} and a low value ranging from 0 to 60.

C. Dynamic Behavior

1) Dynamic model: The dynamics of a droplet driven by EHD is non linear and the behavior is highly dependent of the viscosity of the liquid, where the regimes can be dominated by the viscous effect or by the inertia, called overdamped or underdamped regimes respectively [22].

As the liquid used for the experiment has a high viscosity (glycerine), it can be considered that it behaves in the overdamped regime [37] (Reynolds number $\approx 5 \times 10^{-3} << 1$). In this regime, the time constant τ it is also non linear, and depends on the size of the droplet, viscosity, and the changes in contact angles (voltage applied [22]), and also the contact line pinning [38]. In this work, to reduce the complexity of the model, we propose to model the dynamics of the height of the droplet as a first order system with a constant τ . This model has the time response to a step given by equation (7), and the transfer function (8) where τ is the time constant, h_{ss} is the steady state value and t the time.

$$h(t) = h_{ss}(1 - e^{-\tau/t}) \;, \qquad G(s) = \frac{1}{\tau s + 1} \qquad (7,\, 8)$$

2) Dynamic response: The dynamics of electric field-driven droplets is complex and can differ depending on whether the droplet is wetting or dewetting, as well as its dependence on the contact angle. Therefore, the dynamic response in the wetting and dewetting regimes were explored separately and for several types of voltage signal and ranges.

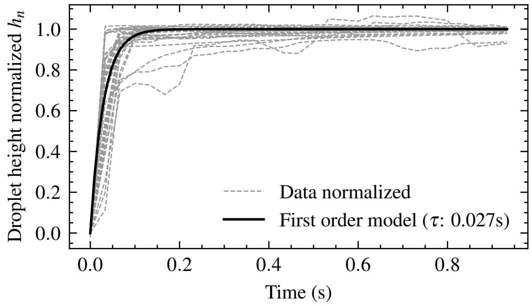

Fig. 8. Normalized data of the time response to different step inputs in the wetting and dewetting regime. The red line shows the identified model response. The data was normalized by the initial and the steady state value $h_n(t) = (h(t) - h_0)/(h_{ss} - h_0)$.

To characterize the dynamic response of the system within our range of actuation, two types of staircases with variable-amplitude signals were employed as input. The first signal maintains a constant low value of 0 V, while the high value of the signal increases from 0 to 60 V in steps of $\Delta U = 2.5$ V_{rms}. The advancing and receding regimes are shown at the top of Figure 7a. The second signal maintains a constant high value of 60 V, while the low value of the signal decreases from 60 to 0 V in steps of $\Delta U = -2.5$ V_{rms}, with the advancing and receding regimes shown at the top of Figure 7b.

The dynamic response of each signal was separated into receding and advancing regimes. The results are shown in Figure 7. In these figures, we can see that all the curves show an overdamped behavior. Moreover, in all the cases tested, 90% of the steady-state value is reached in less than 0.22 seconds, which is compatible with our goal of using droplets

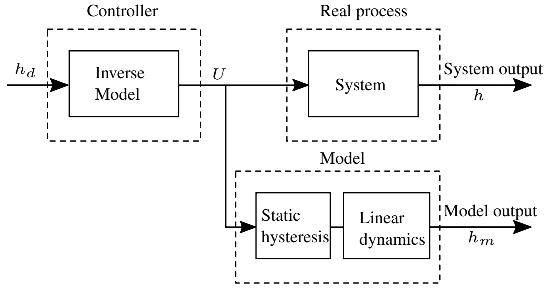

Fig. 9. Schematics of the control loop proposed. The input is the desired height of the droplet h_d, the controller is the inverse of the static model, which provides the voltage U to reach the desire value, and the output is the actual value of the height of the droplet h.

actuated by EHD as fluid joints.

Finally, all these curves were normalized with the height change and the data were fitted to the first-order model proposed in equation (7), obtaining a time constant (τ in Equation 8) of 0.027 seconds. The results are shown in Figure 8. In this figure it is noted that some cases present a slower dynamics. This error in the model can be attributed to the assumption that τ is constant, as it is influenced for voltage applied. One way to mitigate this would be by considering its value depends on the voltage $\tau = \tau(U(t))$. However, almost 95% of the data falls within the 10% error band.

IV. OPEN LOOP HEIGHT CONTROL

Having developed models of the droplet, we explore open-loop control in this section. To control the height of the droplet, an open loop control system as in Figure 9, was utilized and implemented as in Figure 2. The input of this control loop is the desired height, h_d, and the output the actual height of the droplet h. As controller, an inverse model of the static hysteresis presented in section III-B1 was used. This controller provides the voltage necessary to reach the desired height. The model inversion was made by separating firstly in advancing and receding regimes, and then by using linear interpolation on a set of points calculated using the direct model.

As set points, 20 values were randomly defined between 1000 and 1150 μm. The voltages necessary to reach these set points were then calculated by inverting the previously proposed model. Each set point was maintained for a duration of 5 seconds and this experiment was repeated six times. In Figure 10, the results of the open-loop control are presented, along with the error between model and visual feedback, and three snapshots of the actuation. In addition, a video of the actuation is attached to the article. In the top plot of the figure, the model simulation is shown in red, and the measured data is presented in black. Since the data measurements were conducted multiple times, the dotted line in the figure represents the mean, while the shaded areas denote the error band, calculated as the standard error of the measurements.

We can see that the data measure successfully follows the set points with a steady-state error less than 14 μm (9.3% of full range). Also, we can notice that the biggest errors in the steady state are when the height is high, which means when the voltage is low, and the droplet moves in the receding regime. This agree with the model fitting where we can see in Figure 6, that biggest errors in the fitting are at low voltages in the receding regime. Regarding the transient response, we can see that there is an important difference with the model when the height is high, showing slower dynamics. This is due to the linearity of the model which does not take into account that the dynamic response changes with the height of the droplet. Additionally, the fact that this experiment has been performed several times and that the same response has been obtained, demonstrates the repeatability of the process.

V. CONCLUSIONS

In this work, we modeled, designed, characterized, and successfully demonstrated an open-loop control of a droplet's height driven by electrohydrodynamics forces. The model proposed consisted of a steady-state model and a linear first-order dynamics. The steady-state model was based on the energy of system taking into account the surface and electrical energy, and also considering the pinning of the contact line.

The droplet positioning prediction was successfully tested using several electrodes designs. Moreover, using a 3 μL droplet of glycerine a selected device was characterized when a voltage is applied in the electrodes. Through the characterization of the actuator motion range and its signal frequency dependence, the signal frequency was set at 200 Hz.

The system exhibited an hysteresis loop response and a range of actuation of 150 μm was reached with a voltage of 60 V_{rms}. The device achieves approximately ten times greater actuation range compared to electrothermal MEMS of similar size, as in [39], and devices with comparable actuation ranges in conventional electrothermal MEMS requires sizes ten times larger [40]. The actuator designed in all tested cases reaches 90% of the steady value in less than 0.22 seconds and without overshoot. The proposed model was fitted with experimental data and inverted using linear interpolation. In the open loop control, we used the inverted model as a controller. Finally, the model and control proposed was tested using randomly generated set points and we found that the maximum error in the height was less than 14 μm, which means less than 10% of its maximum range, and verify that the proposed models enables to control the droplet in open loop. Furthermore, a repeatable actuation of more than 100 times was verified.

In future work, the accuracy and robustness of the control system can be improved by using visual feedback and closed-loop control. The strength of using capillary forces is that its effects govern the droplet physics down to sub-micrometer scale. Therefore, miniaturization of the proposed actuator and its control model while guaranteeing a large actuation range compared to the size is straightforward. For this, future work will focus on downscaling the proposed system while increasing in relative actuation range by reducing the size of the electrodes and the volume of the droplet. Moreover, thanks to the already embedded electrodes, impedance measurement can be explored to integrate actuation and measurement in one compact device.

This droplet height control system is the first step toward the use of fluid joint based linear actuators or to actuate singles

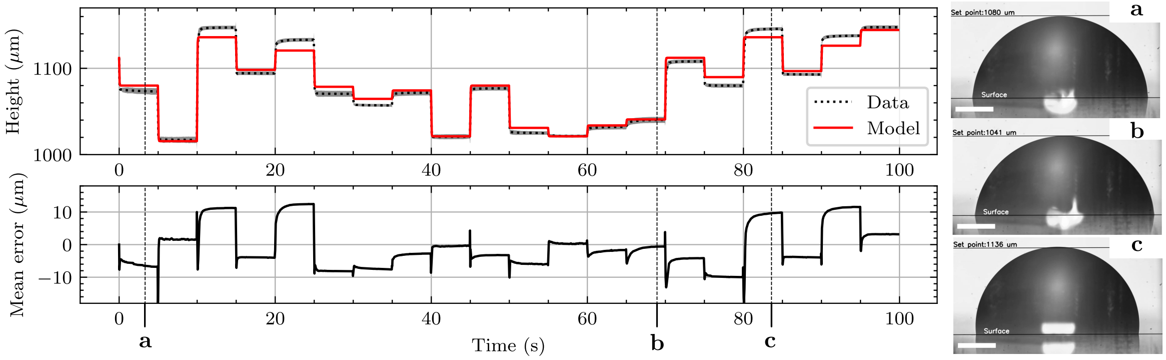

Fig. 10. Results of the open-loop height control of 20 randomly generated setpoints, conducted six times. The red line represents the model prediction, the dotted black line illustrates the measured data, with its shadow indicating the standard deviation, and the solid black line represents the mean error of the model. The following images provide side-view snapshots of the actuation, with lines representing the set point and the electrode surface (scale bar, 500 μm).

platforms or parallel robots with micrometric dimensions. Moreover, this control approach can be used in a mirror plate driven by droplets as in [17]. In the near future, this type of actuator will be applied to drive a parallel robot with three fluid joints.

Acknowledgments

This work has been supported by the EIPHI Graduate School (contract ANR-17-EURE-0002), by the Bourgogne Franche-Comté region through the ConAFlu project, by French RENATECH network and its FEMTO-ST technological facility, by the French ROBOTEX network and its Micro and Nanorobotics center under Grant ANR-10-EQPX-44-01, by the ANER project ROBOCAP funded by the Bourgogne Franche-Comté region and ANR E-wetBot project Projet-ANR-22-CE33-0011.

References

[1] P. Lambert, *Capillary forces in microassembly: modeling, simulation, experiments, and case study*. Springer Science & Business Media, 2007.
[2] T. Ito *et al.*, "Vision feedback control for the automation of the pick-and-place of a capillary force gripper," *Micromachines*, 2022.
[3] B. Chang *et al.*, "Capillary pick-and-place of glass microfibers," *IEEE Access*, 2021.
[4] W. Hagiwara *et al.*, "Capillary force gripper for complex-shaped micro-objects with fast droplet forming by on–off control of a piston slider," *IEEE Robotics and Automation Letters*, 2019.
[5] F. N. Piñan Basualdo *et al.*, "A microrobotic platform actuated by thermocapillary flows for manipulation at the air-water interface," *Science robotics*, 2021.
[6] J. Yuan *et al.*, "Dielectrowetting control of capillary force (cheerios effect) between floating objects and wall for dielectric fluid," *Micromachines*, 2021.
[7] A. Barbot *et al.*, "Exploiting liquid surface tension in microrobotics," *Annual Review of Control, Robotics, and Autonomous Systems*, vol. 6, pp. 313–334, 2023.
[8] M. De Volder *et al.*, "A novel hydraulic microactuator sealed by surface tension," *Sensors and Actuators A: Physical*, 2005.
[9] A. Barbot *et al.*, "Liquid seal for compact micropiston actuation at the capillary tip," *Science advances*, 2020.
[10] C. Lenders *et al.*, "Three-dof microrobotic platform based on capillary actuation," *IEEE transactions on robotics*, 2012.
[11] F. N. P. Basualdo *et al.*, "Pose control of millimeter-scale objects in a laser-powered thermocapillary manipulation platform," *IEEE/ASME transactions on mechatronics*, 2023.
[12] C. Maggi *et al.*, "Micromotors with asymmetric shape that efficiently convert light into work by thermocapillary effects," *Nature communications*, 2015.
[13] A. Takei *et al.*, "Capillary motor driven by electrowetting," *Lab on a Chip*, 2010.
[14] J. Kedzierski and E. Holihan, "Linear and rotational microhydraulic actuators driven by electrowetting," *Science Robotics*, 2018.
[15] Z. Cenev *et al.*, "Ferrofluidic manipulator: Automatic manipulation of nonmagnetic microparticles at the air–ferrofluid interface," *IEEE/ASME Transactions on Mechatronics*, 2021.
[16] B. Daunay *et al.*, "Effect of substrate wettability in liquid dielectrophoresis (ldep) based droplet generation: Theoretical analysis and experimental confirmation," *Lab on a Chip*, 2012.
[17] I. Frozanpoor *et al.*, "Tilting micromirror platform based on liquid dielectrophoresis," *Sensors and Actuators A: Physical*, 2021.
[18] Q. Ni *et al.*, "Open-loop electrowetting actuation with micro-stepping," *Sensors and Actuators A: Physical*, 2016.
[19] R. Casier *et al.*, "Position measurement/tracking comparison of the instrumentation in a droplet-actuated-robotic platform," *Sensors*, 2013.
[20] A. Vasudev and J. Zhe, "A low voltage capillary microgripper using electrowetting," in *TRANSDUCERS 2009-2009 International Solid-State Sensors, Actuators and Microsystems Conference*. IEEE, 2009.
[21] A. O. Ashtiani and H. Jiang, "Design and fabrication of an electrohydrodynamically actuated microlens with areal density modulated electrodes," *Journal of Micromechanics and Microengineering*, 2015.
[22] K. Xiao and C.-X. Wu, "Droplet dynamics driven by electrowetting," *Phys. Rev. E*, vol. 105, p. 064609, Jun 2022.
[23] R. Zhao *et al.*, "Contact angle hysteresis in electrowetting on dielectric," *Chinese Physics B*, 2015.
[24] M. Mastrangeli, "The fluid joint: The soft spot of micro-and nanosystems," *Advanced materials*, 2015.
[25] C. Qi *et al.*, "Electrohydrodynamics of droplets and jets in multiphase microsystems," *Soft Matter*, 2020.
[26] F. Mugele and J.-C. Baret, "Electrowetting: from basics to applications," *Journal of physics: condensed matter*, 2005.
[27] I. Frozanpoor *et al.*, "Continuous droplet-actuating platforms via an electric field gradient: electrowetting and liquid dielectrophoresis," *Langmuir*, 2021.
[28] W. Wang *et al.*, "Observation of contact angle hysteresis due to inhomogeneous electric fields," *Communications Physics*, 2021.
[29] P. Lambert, "Surface tension in microsystems: Engineering below the capillary length," *Surface Tension in Microsystems*, 2013.
[30] N. Majcherczyk *et al.*, "Experimental characterization of drobot: Towards closed-loop control," in *2014 IEEE/ASME International Conference on Advanced Intelligent Mechatronics*. IEEE, 2014.
[31] G. Launay, "PyDSA: Drop shape analysis in Python," 2018–, [Online; accessed 22-11-2023].
[32] Y.-S. Yu *et al.*, "Experimental and theoretical investigations of evaporation of sessile water droplet on hydrophobic surfaces," *Journal of colloid and interface science*, 2012.
[33] C. G. Cooney *et al.*, "Electrowetting droplet microfluidics on a single planar surface," *Microfluidics and Nanofluidics*, 2006.
[34] J. S. Sharp, "Resonant properties of sessile droplets; contact angle dependence of the resonant frequency and width in glycerol/water mixtures," *Soft Matter*, 2012.
[35] K. A. Brakke, "The surface evolver," *Experimental mathematics*, 1992.
[36] H. Verheijen and M. Prins, "Reversible electrowetting and trapping of charge: model and experiments," *Langmuir*, 1999.

[37] Q. Vo *et al.*, “Universal transient dynamics of electrowetting droplets,” *Scientific reports*, 2018.

[38] Y. Lu *et al.*, “Dynamics of droplet motion induced by electrowetting,” *International Journal of Heat and Mass Transfer*, vol. 106, pp. 920–931, 2017.

[39] M. Saqib *et al.*, “Design and analysis of a high-gain and robust multi-dof electro-thermally actuated mems gyroscope,” *Micromachines*, 2018.

[40] C. Nakic *et al.*, “Development of an electrothermal micro positioning platform for laser targets with two degrees of freedom,” in *2016 International Conference on Manipulation, Automation and Robotics at Small Scales (MARSS)*. IEEE, 2016.

Francisco Ortiz received the B.Eng. degree in mechanical engineering and an M.S. degree in engineering from Balseiro Institute, Argentina, in 2019 and 2021. He is currently pursuing his PhD degree in Robotics at UBFC, France, and is a member of the Automatic Control and Micro-Mechatronic Systems Department of the FEMTO-ST Institute in Besancon, France. His main research interests are microrobotics and actuation based on surface tension forces.

Aude Bolopion received her Ph.D. degree in robotics in 2010 from Sorbonne University (ex. Pierre et Marie Curie University), Paris, France. She was a member of the ISIR Institute. Her research interests are focused on microrobotics and micromanipulation. She got a CNRS researcher permanent position at the FEMTO-ST Institute, Besancon, France in 2011. She received the CNRS bronze medal in 2019 for her work on non contact actuation for microrobotics.

Antoine Barbot received the Ph.D. degree in robotics from the Centre for Nanosciences and Nanotechnologies-French National Centre for Scientific Research (CNRS), Paris, France, in 2016.,He was a Postdoctoral with Imperial College London, London, U.K., where he focused on microrobotics applied to noninvasive surgery. He particularly developed floating magnetic microrobots for flexible microelectronic assembly and also micropneumatic and microfluidic actuators embedded at a capillary tip. Since 2020, he has been a CNRS Researcher with Franche-Comté Électronique Mécanique Thermique et Optique - Sciences et Technologies Institute, Besançon, France. His research focuses on capillary force for microrobotics.